PHILOSOPHICAL TRANSACTIONS A

rsta.royalsocietypublishing.org

Research

Article submitted to journal

Subject Areas:
solid-state chemistry, material physics, low temperature physics, crystallography, frustrated magnetism

Keywords:
magnetocaloric, correlated disorder, metal-organic framework, emergent order

Author for correspondence:
P. J. Saines
e-mail: P.Saines@kent.ac.uk

Emergent magnetic order and correlated disorder in formate metal-organic frameworks

R. J. C. Dixey[1], F. Orlandi[2], P. Manuel[2], P. Mukherjee[3], S. E. Dutton[3] and P. J. Saines[1]

[1]School of Physical Sciences, Ingram Building, University of Kent, Canterbury, CT2 7NH, United Kingdom
[2]ISIS Facility, STFC Rutherford Appleton Laboratory, Chilton, Didcot, OX11 0QX, United Kingdom
[3]Cavendish Laboratory, University of Cambridge, JJ Thomson Avenue, Cambridge CB3 0HE, United Kingdom.

Magnetic materials with strong local interactions but lacking long range order have long been a curiosity of physicists. Probing their magnetic interactions is crucial for understanding the unique properties they can exhibit. Metal-organic frameworks have recently gathered more attention as they can produce more exotic structures, allowing for controlled design of magnetic properties not found in conventional metal-oxide materials. Historically, magnetic diffuse scattering in such materials have been overlooked but has attracted greater attention recently, with advances in techniques. In this study we investigate the magnetic structure of metal-organic formate frameworks, using heat capacity, magnetic susceptibility and neutron diffraction. In $Tb(DCO_2)_3$ we observe emergent magnetic order at temperatures below 1.2 K, consisting of two **k**-vectors. $Ho(DCO_2)_3$ shows diffuse scattering above 1.6 K, consistent with ferromagnetic chains packed in a frustrated antiferromagnetic triangular lattice, also observed in $Tb(DCO_2)_3$ above 1.2 K. The other lanthanides show no short or long range order down to 1.6 K. The results suggest an Ising-like 1D magnetic order associated with frustration is responsible for the magnetocaloric properties, of some members in this family, improving at higher temperatures.

THE ROYAL SOCIETY PUBLISHING

1. Background

Magnetic materials have long been studied from a fundamental standpoint [1] and for their functional properties, including data storage and transfer, [2] magnetic refrigeration [3] and as MRI contrast agents. [2,4] Ferromagnetism has been known about before modern science through the naturally occurring iron containing mineral, magnetite, [5] despite a lack of understanding of its underlying microscopic magnetic mechanisms. Strong magnetic interactions in oxide materials give rise to high ordering temperatures, but they prevent the appearance of more exotic states of matter. Such exotic states, such as spin liquids and other phases devoid of long range order, are of great interest to the condensed matter community, for the unique phenomena they exhibit.

Metal-organic frameworks (MOFs) may be the ideal systems to search for such exotic states. MOFs have attracted much attention in recent years for the ability to exhibit a wide array of structures and properties, lending themselves to gas storage [6] where design and synthesis of highly porous frameworks is possible. [7] Recently however, magnetic studies of MOFs have emerged, highlighting the potential of magnetic metal-organic frameworks in functional magnetic materials. MOFs have already been shown to exhibit a range of magnetic properties, with uses in chemical and magnetic sensors, [8] magnetocalorics [9,10] and multiferroics that combine magnetism with ferroelectric order. [11]

The ability for greater flexibility in the design of MOFs, allows for more specific topologies and magnetically isolated sheets and chains, opening up the means to low dimensional and frustrated magnetism. In MOFs, the magnetic interactions are facilitated through the connecting ligand, or single anion where the strength and direction of these magnetic interactions depend on the precise nature of the linker. Magnetic interaction strength is typically inversely proportional to the size of the ligand and therefore, in magnetic MOFs, linkers must be kept short to allow sufficient metal-metal magnetic interactions in the dimensions they are desired.

(a) Frustrated magnetism and magnetic systems

To fully understand how frustration can occur the models of magnetism must first be considered, and here the most prevalent models are shown. The simplest model for nearest neighbour magnetic interactions is the Heisenberg model given by the Hamiltonian: $\hat{H} = -\sum_{(i,j)} J_{ij}\vec{S}_i \cdot \vec{S}_j$ where i and j are spin sites on a periodic lattice. $\vec{S}$ is a unit vector, representing the magnitude and direction of a magnetic moment, and J_{ij} is the strength of the interaction between neighbouring spins. In this simplest model, spins are considered to be three dimensional and can be oriented in any direction. Alternatively, spins can be fixed so they can only point up or down along a single axis, known as the Ising model, [12] or in a easy plane - the XY model.

Below some temperature (T_c) the J exchange interactions are sufficient to overcome the thermal fluctuations in the material, and spins can align in a energetically favourable orientation. When the exchange integrals J_{ij} are negative, the spins align anti-parallel to nearest neighbours (antiferromagnetic) (Figure 1a); when exchange integrals are positive the spins are parallel (ferromagnetic). On a square lattice, with no next nearest neighbours, either of these ground states can be satisfied.

Frustration can only occur if there are competing magnetic interactions, usually when some of the exchange paths are antiferromagnetic, if only nearest neighbour interactions are considered. The classical example of these systems are Ising antiferromagnetic coupled spins arranged on a triangular lattice (Figure 1b), first studied by Wannier in 1950. [13] In this model system, it is energetically favourable for the spin to be anti-parallel, with respect to its nearest neighbour, but the crystallographic structure of the materials means there are two near neighbours competing for anti-parallel alignment.

In an Ising system it is not possible to satisfy both simultaneously and so a frustrated ground state emerges with many degenerate energy levels. In a Heisenberg system this frustration can be alleviated though other routes as shown in Figure 1c. When frustration arises purely from the

topology of the lattice, this is described as geometrically frustrated. Whilst this is a convenient illustrative example, frustration is not limited to two dimensions, or even triangular lattices, for example in three dimensions this corresponds to a pyrochlore motif.

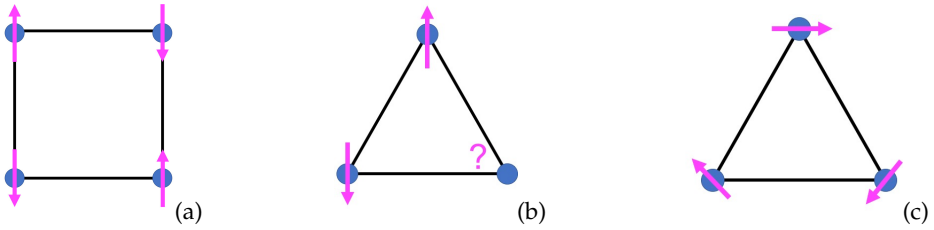

Figure 1. (a) Antiferromagnetically ordered square lattice, (b) a frustrated antiferromagnet on a triangular lattice (c) antiferromagnetically coupled Heisenberg spins on a triangular lattice.

Frustration in materials can lead to exotic states including some of the most studied pyrochlore spin ice materials, $Dy_2Ti_2O_7$ and $Ho_2Ti_2O_7$, consisting of four ferromagnetically coupled lanthanide ions with strong Ising character. [14] Spin ices are named because of their analogy with water ice, with two spins facing the center, and two facing outwards (see Figure 2a). This leads to some fascinating properties, such the existence of magnetic monopoles quasiparticles, [15] that cannot exist in isolation. Spin ice materials are an example of systems which can exhibit magnetically charge ordered states, when one of the spin is flipped. The garnet lattice consists of cations sitting on the vertices of corner sharing triangles, forming a highly frustrated 3D system of interpenetrating rings. Frustration, in the benchmark magnetocaloric $Gd_3Ga_5O_{12}$ garnet (GGG), prevents long range order forming, but shows spin-liquid behaviour between 140 mK and 5 K, [16] where despite significant antiferromagnetic interactions the magnetic moments continue to fluctuate. Unlike a paramagnet however, the spins are correlated and do not form static order even at absolute zero.

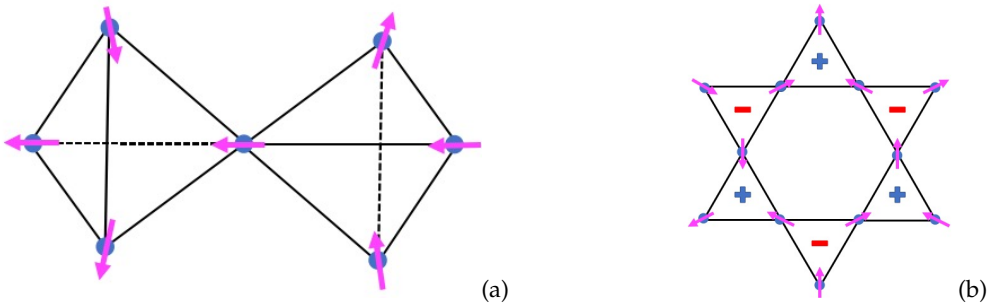

Figure 2. (a) A spin ice tetrahedra with two in, two out spin arrangement (b) a kagome emergent charge ordered state.

By magnetically isolating the layers in crystal lattices from one another, the magnetic order can be reduced to two dimensions, shown in Figure 3. The highly studied two dimensional kagome lattice can be described as a pattern of corner sharing triangles and the triangular lattice is a tessellation of edge sharing triangles with magnetic cations sitting on the vertices. The kagome lattice $Dy_3Mg_2Sb_3O_{14}$ has also shown evidence of emergent charge order (ECO), [17] which displays long range magnetic order, on average, not present on the local scale due to frustration (see Figure 2b). This has been described as magnetic fragmentation i.e. the system can be thought of as in two states: a divergence free state (which gives rise to Bragg Scattering) and a divergence

full state (which is the origin to the diffuse scattering and the kagome and pyrochlore pinch points). The unequal in/out arrangement of spins on the triangle create magnetic dipoles, which can be considered analogous to electric charges. Like electric charges, the magnetic charges repel and attract opposites, and so are forced to arrange into the lowest possible energy state. [17]

For the two dimensional case, the triangular lattice is the simplest case which can accommodate frustration, one such example is the yavapaiite mineral with the general structure $AM(SO_4)_3$. The alkali metal A cation layers isolate the layers of magnetic ions, so the ground state magnetic order is constrained to two dimensions. Magnetic order $CsFe(SO_4)_2$ and $RbFe(SO_4)_2$, relieves frustration through antiferromagnetically coupled spins rotated by 120° in the *ab* plane, [18] which is only possible in the case because the spins are Heisenberg-like. [19] An Ising system, with a single easy axis, cannot relieve frustration through this method. Long range order is suppressed due to competing interactions, but unlike a paramagnet the spins are strongly correlated with their immediate neighbouring spins. [20]

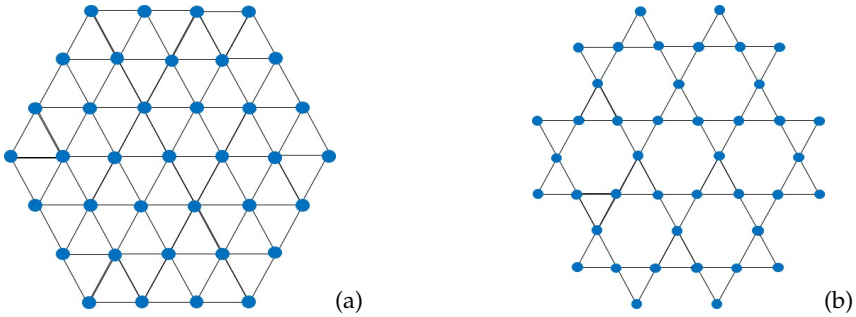

Figure 3. Two 2D geometrically frustrated crystal structures. (a) The triangular lattice - edge sharing triangles (b) The kagome lattice - corner sharing triangles.

The kagome lattice is well studied, for its high degree of frustration, its potential as a quantum spin-liquid (QSL) state [21] and the variety of minerals whose transition metal ions form such a lattice. QSLs form a novel class of matter where despite strong interactions between neighbouring spins, the system does not form any long range order, due to (zero-point) quantum fluctuations. [22] The first experimentally observed QSL candidate was in the mineral Hebertsmithite in 2006. [23] Interest has re-emerged in QSLs since the discovery of Majorana fermions in the QSL α-$RuCl_3$ [24] - a type of particle that is it's own anti-particle and does not obey the Dirac equations. First predicted in 1937 [25] but only recently experimentally observed, has opened up new horizons in condensed matter physics. QSL candidates can also be found in the triangular lattice $YbMgGaO_4$, consisting of highly disordered correlated Ising spins. [26]

(b) 1D Magnetism

When the exchange interactions between magnetic ions is restricted to one dimension the material behaves as a 1D system. Such systems have attracted great interest for the potential to discover new phases of matter, attracting interest for quantum information transfer [27] and spin quasi-particles. [28] Long range 1D magnetic order cannot exist in an isolated system, with the exception of an Ising system exclusively at 0 K due to a spin gap. [29] For an isolated 1D Ising ferromagnet, with a ground state of -$nJ/2$, where n (the number of magnetic ions in the chain) is very large, a defect in the chain has an energy cost of $J/2$. However, the entropy gain is equal to $\kappa_b \ln n$, thereby any defect introduced into the system by a magnetic or temperature fluctuations, [30] will induce a response throughout the chain.

Examples of low dimensional magnetism do exist, but it's often difficult in mineral and oxide systems to properly isolate magnetic chain from interacting with each other. While this is far from

an exhaustive list, [31] some examples of this include the $AFeX_3$ family of compounds (where A = Rb or Cs and X = Cl or Br) consisting of stacked triangular lattices. These systems behave as Heisenberg quasi-1D spin chains, and in the case of $CsFeCl_3$ does not show any long-range 3D order down to 0.8 K. [32] If chains are poorly isolated as is the case for $RbFeCl_3$, the material will transition to a 3D ordered state. [32]

In the extended perovskite ABX_3 family other examples of quasi-1D magnetic compounds include $CsNiF_3$ and $CsCuCl_3$, with the latter being extensively studied. Both have their own associated fascinating ground state physics, but still consist of stronger Heisenberg ferromagnetic correlations in 1D with weaker antiferromagnetic exchange between the ferromagnetic chains. [33,34] An interesting result in 1D magnetism can be found in the compounds Sr_3CuIrO_6 and Sr_3CuPtO_6, which are 1D Heisenberg ferromagnetic and antiferromagnetic, respectively. Mixing of the two materials results in a random ferro/antiferromagnetic paramagnetic state, described as a quantum spin chain paramagnet. [35]

More fascinating examples of quasi-1D systems are the Ising 1D systems. $Ca_3Co_2O_6$ has been extensively studied experimentally and theoretically as it undergoes a transition to 1D magnetic state in zero field and contains unusual magnetic properties. [36,37] It has 1D ferromagnetic intrachain correlations and weaker interchain antiferromagnetic interactions, and at low temperatures orders into longitudinal amplitude-modulated spin-density wave (SDW) propagating along the c-axis. α-CoV_2O_6, a 1D Ising ferromagnet, [38] undergoes transitions into different phases under variable applied fields. Studies of this material also showed that it was an excellent magnetocaloric, within it's operating temperature, with a steep magnetisation curve as a result of overcoming the antiferromagnetic interchain correlations into a ferromagnetic state. It should be noted that these systems show quasi-1D Ising like behaviour only because they are not truly isolated 1D chains, and exhibit 3D magnetic order.

For highly frustrated or low dimensional materials, with only short-range order, the correlated disorder may materialise as structured diffuse scattering [20]. With modern advances in understanding of magnetic systems and new reverse Monte Carlo (RMC) techniques it is now possible to probe the nature of this diffuse scattering from powder neutron diffraction experiments. [39,40]

(c) Exotic Magnetism in Metal-Organic Frameworks

All examples discussed so far, are dense oxides and minerals but the greater flexibility in design of the size, shape and coordination of organic linkers in MOFs allow for more complex magnetic structure and the ability to tailor desired magnetic properties. Forming one or two dimensional magnetic systems in oxides is not trivial, exemplified by the scarce physical realisations of theoretical models in these exotic states of matter. MOFs are a good alternative because they can have longer distances between magnetic centers, and therefore can better isolate the magnetic sheets or chains from each other. However, these low dimensional units can remain strongly coupled through oxygen atoms. It is possible to modify the ligand to achieve desired exchange interactions, making MOFs an ideal model systems for the study of new physics. Until recently, the field of magnetic MOFs have been largely overlooked and many studies remain limited to bulk magnetic property measurements. There are much fewer detailed studies of the microscopic magnetic phases in MOFs, which typically require neutron based techniques to characterise in detail. [41]

Examples of exotic magnetism in MOFs are present in the literature including chiral, 2D and 1D magnetic structures, in addition to long range magnetically ordered systems. [41] Frustrated magnetism has been experimentally studied in magnetic MOFs in materials such as $Co_3(OH)_2(sq)_2.3H_2O$ and $M(tca)_2$ (tca = tricyanomide), using neutron scattering but these materials undergo phase transitions to 3D long-range ordered structures, at low temperature. $Co_3(OH)_2(sq)_2.3H_2O$ has significant frustration within its CoO_6 ribbons, and unusually undergoes a phase transition upon dehydration. [42] In Mn(tca) strong frustration is observed and is relieved by the formation of an incommensurate 3D structure. [43]

$Tb(DCO_2)_3$ is an excellent example of a magnetic MOF with interesting properties at low temperatures and a physical realisation of a stacked triangular lattice, forming chains of Tb ions (Figure 4). The material perfectly combines frustration and 1D magnetic order, [44] making it the ideal model for the triangular lattice with equivalent J coupling between Tb ions, through the formate ligand. The MOF examples discussed so far all have 3D ordered ground states but, for this Ising antiferromagnetic compound, the situation appears to be different. Above 1.6 K it shows strong magnetic diffuse scattering as a result of short range order emerging from ferromagnetically correlated chains, coupled through frustrated antiferromagnetic interactions on the triangular lattice. Below 1.6 K it displays long range Ising-like 1D magnetic order along the c-axis with spins aligned in the chain direction, but shows no long range order in the ab plane. The lack of long range 3D order appears to be suppressed by the frustrated interactions between chains leading to the emergence of a triangular Ising antiferromagnetic (TIA) state, with a large number of degenerate ground states. [44] The ferromagnetic correlations and antiferromagnetic frustration that persists, in the paramagnetic state, allow for high entropy changes in small applied magnetic fields contributing to a high efficiency as a magnetocaloric. [9] This dominant ferromagnetic intrachain coupling allow the moments to be more easily aligned with the applied field. The additional weaker frustrated antiferromagnetic interchain interactions lead to suppression of magnetic order, in absence of a field, required for paramagnetic magnetocalorics. This study aims to expand on the studies of $Tb(DCO_2)_3$ thus far, exploring the magnetic structure between 0.28 and 1.95 K and physical property measurements to lower temperatures to establish how the TIA phase is modified. The other compounds in the $Ln(DCO_2)_3$ series are also probed by neutron diffraction for diffuse scattering indicative of short-range magnetic correlations.

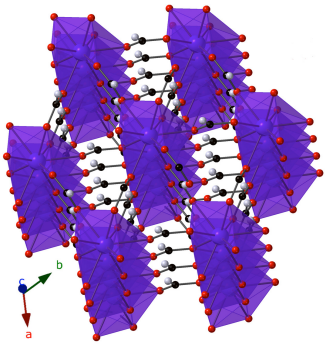

Figure 4. $Tb(HCO_2)_3$ crystal structure. Tb^{3+} coordination environments are shown as purple polyhedra, and carbon, oxygen and hydrogen are shown in black, red and white respectively.

2. Experimental Methods

$Ln(HCO_2)_3$ and $Ln(DCO_2)_3$ (where Ln = Ce, Pr, Nd, Tb-Er) samples were synthesized by slowly adding 2 g of $Ln(NO_3)_3.6H_2O$ (99.9%, Sigma-Aldrich) to a solution of 4.75 mL of formic acid (97.5% Sigma-Aldrich), or d-formic acid (95.0% Sigma-Aldrich), respectively, with 0.25 mL of ethanol added. After several minutes of stirring, NO_x was released and the product precipitated out of solution. The products were collected by vacuum filtration, washed several times with ethanol, and dried in a desiccator. It is necessary to deuterate neutron samples to minimise background noise caused by the incoherent scattering of hydrogen.

Powder neutron diffraction measurements were carried out on the high-resolution time-of-flight (TOF) WISH diffractometer at the ISIS neutron source, Rutherford Appleton Laboratory. [45] $Tb(DCO_2)_3$ measurements were carried out between 0.28 K to 1.95 K, with the sample cooled using a ^{3}He Heliox sorption refrigerator. $Ln(DCO_2)_3$ (where Ln = Ce, Pr, Nd, Dy, Ho and Er)

measurements were carried out between 1.6 K to 100 K, with the samples cooled using the standard Oxford Instruments WISH cryostat. Average structure neutron patterns were fitted in FULLPROF [46] and JANA2006 [47] using the Rietveld method. [48] The base temperature solution was determined using JANA2006 and the evolution of the magnetic moments with respect to temperature was fitted in FULLPROF. Diffuse neutron patterns were fitted with the reverse monte carlo program - SPINVERT, [40] using a supercell of 52 x 54 x 55 $Å^3$. Heat capacity measurements were measured on a Quantum Design PPMS DynaCool with 14 T superconducting magnet and ^{3}He insert, between 400 mK and 14 K. The 400 mK - 30 K magnetic measurements of the polycrystalline samples were performed using a Quantum Design MPMS SQUID magnetometer, with a ^{3}He insert in a 100 Oe DC magnetic field. For additional details see the supplementary appendix 1.

3. Results and Discussion

(a) Magnetic Properties of $Tb(HCO_2)_3$ framework

It has previously been reported that the $Ln(HCO_2)_3$ frameworks do not show any indication of long range order down to 2 K, and follow Curie-Weiss behaviour, with Weiss temperatures of -0.6 K, -0.9 K, -6.1 K, -10.3 K and -16.0 K, for *Ln* = Gd–Er. [9] Since neutron diffraction measurements indicated the emergence of magnetic order in $Tb(HCO_2)_3$ at 1.6 K we have probed the physical properties down to 0.4 K to identify the effect this order has on it's physical properties. Zero-field cooled (ZFC) magnetic susceptibility data for $Tb(HCO_2)_3$ shows indications of magnetic transitions at ≈1.6 K and ≈0.5 K, (see Figure 5). Heat capacity measurements shown in Figures 5b and S1 show a have a large peak in 1.68 K for zero applied field, this is suppressed in applied fields consistent with the onset of a magnetic transition. Despite the small change in susceptibility, associated with the TIA transition, the signal in heat capacity is much more significant. Both of these features are consistent with the emergence of the TIA, as a transition to a long range 1D order would result in a large entropy change, while the strong short range antiferromagnetic coupling of the chains would prevent any great change in magnetic susceptibility. It is also possible that the signal at 1.6 K is an experimental artefact from the MPMS switching between high and low temperature modes. A clearer transition can be seen at ≈0.5 K indicating more complete, possibly long-range antiferromagnetic order. [9,44] A second large change in the heat capacity is observed below 600 mK, this may be the onset of long-range order but could also be the onset of a hyperfine Schottky anomaly.

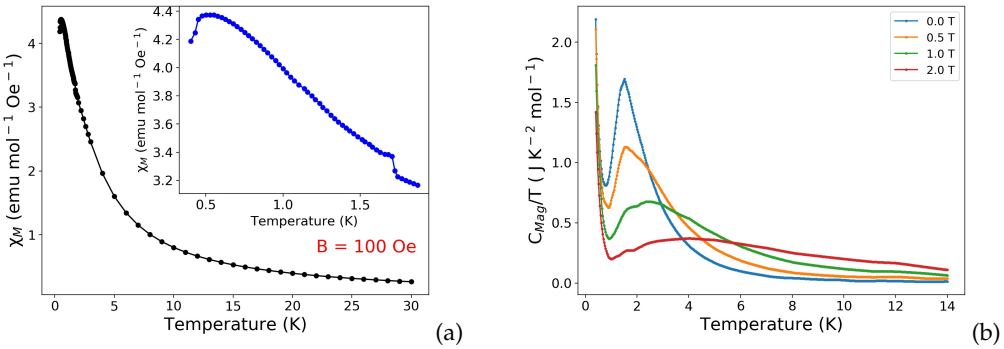

Figure 5. Magnetic measurements of $Tb(HCO_2)_3$. (a) Magnetic susceptibility in 100 Oe field below 30 K, close up below 1.6 K in insert, (b) C_{mag}/T in variable fields between 400 mK and 14 K.

(b) Magneto-structural characterisation of *Ln*$(DCO_2)_3$ frameworks

The interesting physical and magnetic measurements encouraged further investigation, so we have therefore performed neutron diffraction measurements in zero-field of the *Ln*$(DCO_2)_3$ frameworks. Rietveld fits to neutron diffraction data confirmed that all *Ln*$(DCO_2)_3$ samples used in this study were phase pure and did not exhibit significant exchange of D for H. They were all found to adopt the known rhombohedral $R3m$ structure under ambient conditions (see Figure S2-25). [9] In this structure the *Ln*O_9 polyhedra are connected into face-sharing chains down the *c*-axis with these chains interconnected via the formate ligand into a triangular arrangement (see Figure 4). There are two different oxygen atoms in the structure, bonding to one and two Ln^{3+} cations, respectively, with the latter atom connecting the Ln^{3+} cations into chains. The triangle connections of the Ln^{3+} cations are not equilateral but instead feature two short bonds and one long bond, which rotate between adjacent layers along the *c*-axis.

(i) $Tb(DCO_2)_3$

Upon cooling below 1.6 K the neutron diffraction measurement performed on $Tb(DCO_2)_3$ show the appearance of extra reflections ascribable to the development of long range magnetic ordering. This can be appreciated from the broad peak observed around 9 Å(Figure 6b). The extra reflections can be indexed with a propagation vector $\mathbf{k}_1$ = [0,0,1] belonging to the LD line (00γ) of the first Brillouin zone (BZ). The quantitative Rietveld refinement agrees with the $P3m'1$ magnetic space group corresponding to the mLD2LE2 irreducible representation with order parameter (ξ_1,ξ_2) as previously reported. [9]

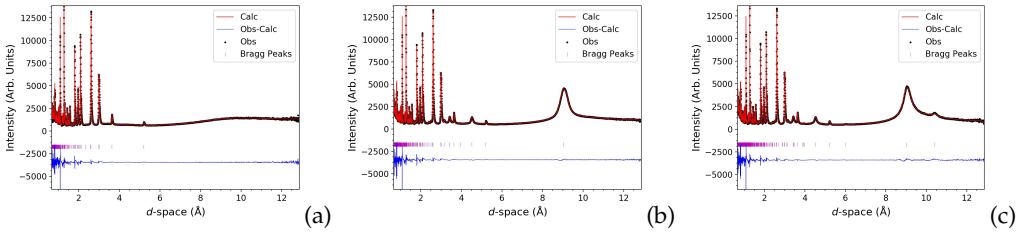

Figure 6. Rietveld fits to neutron diffraction patterns of $Tb(DCO_2)_3$ at variable temperatures from bank 2 and 9 of WISH along with the fitting statistics (a) 1.7 K, R_p = 6.45 %, R_{wp} = 5.27 % (b) 1.2 K, R_p = 6.51 %, R_{wp} = 5.44 % (c) 0.28 K, R_p = 6.58 %, R_{wp} = 5.41%.

It is worth underlining that the observed propagation vector does not correspond to a special point of the BZ and the γ value can, in principle, be incommensurate. The broad nature of the diffraction peaks does not allow us to determine with absolute certainty that the propagation vector is locked to the commensurate [0,0,1] value. Nevertheless the comparison with similar systems in the literature and the good refinement of the diffraction data with the commensurate value let us to conclude that the real propagation vector is likely to be γ=1, as previously reported. [9] The spin ordering can be described two different global phases. One of these resembles a partially disordered antiferromagnet (PDA) in which each of the triangles has one chain ordered up, one down, and the third remaining disordered ($\pi/4$). The other up-down-down model contains one TbO_9 chain ordered up, and two down with the latter having half the magnetic moment of the former ($\pi/6$). [9,49] The two descriptions for the magnetic structure cannot be distinguished between, as they only vary in the phase ($\pi/4$ and $\pi/6$), which diffraction is not sensitive to. As reported previously both of these can thought of as conventional crystallographic approximations of the TIA, which only has long range 1D order in the chains. [44]

Patterns collected below 1.2 K revealed the presence of additional diffuse reflections at high *d*-space, the most significant Bragg-like peak can be seen at ≈10.5 Å. The broad nature of these

features, comparable to those associated with the TIA phase and the retention of the diffuse suggest these are associated with a state that lacks conventional crystallographic order. We have, however, treated them with conventional crystallographic approaches, as in the absence of clearly established prediction of the scattering, we cannot completely exclude that the peak broadening is not a result of small magnetic domains. The peak width was fit with an anisotropic peak broadening model, and the broadening is an indication of a finite correlation length. When fit with a Warren-like peak shape function [50] the correlation length, considered to be associated with correlations in the *ab* plane, was found to be ≈52 Å.

We observed no reduction in the width of the magnetic peaks upon cooling below 1.6 K indicating the magnetic correlation length remains unchanged. These extra reflections can be indexed to a supercell violating the parent rhombohedral symmetry and doubled along the *b*-axis with a $\mathbf{k}_2$-vector = [0,0.5,1] corresponding to the mF2 mode. These new reflections here have been interpreted as an additional component of the magnetic structure, but the possibility of magnetic phase separation in the material cannot be completely excluded. The lack of intensity on the satellites of the *00l* reflections indicate that the moment remains along the *c*-axis only, in agreement with the Ising character of the Tb spins.

Using ISODISTORT [51] we have determined the commensurate structure can be described in the Pm' space group in which there are six independent Tb sites with moments dependant on the global phase, with the lattice parameters *a* = 3.96860(13) Å, *b* = 10.42077(15) Å, *c* = 18.0493(3) Å as shown in figure 7. Since the structure factors are insensitive to the choice of the global phase, it is not possible to distinguish between the two structures from the neutron diffraction alone.

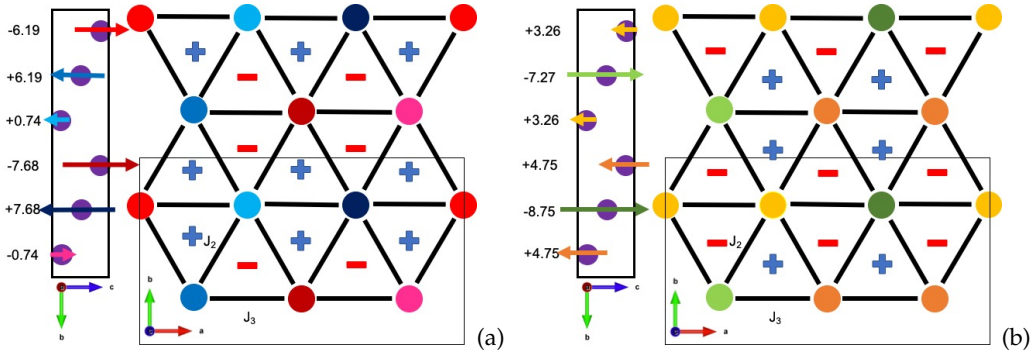

Figure 7. $Tb(DCO_2)_3$ two possible magnetic average structure solutions at 0.28 K. Unit cell shown as black box with magnetic moments in Pm' space group. The spin charges are shown as minus and plus signs. J_2 and J_3 are shown next to the corresponding interaction and J_1 not shown, goes into the plane. On the right of each figure is shown the projection of the structure in the ab plane and on the left of each figure the bc plane. Magnetic moments colour coded, but not to scale. (a) Global phase = $\pi/4$ (b) Global phase = $\pi/6$.

The solution with global phase $\pi/4$ results in a modification of the PDA structure in which the $\mathbf{k}_2$ propagation modulates the moment in the chains resulting in couples of large moment Tb chains ($\pm$7.68(3) μ_B and $\pm$6.19(3) μ_B) anti-ferromagnetically coupled separated by chain with a small moment ($\pm$0.74(3) μ_B). For the high temperature magnetic structure this phase choice gives a partially disordered antiferromagnet solution closest to the TIA model proposed, [44] and therefore is our preferred model. The $\pi/6$ solution, is a slight modification of the up $\frac{1}{2}$down $\frac{1}{2}$down structure on a triangular lattice in which the moments are modulated along the *b*-axis of the parent structure. [49] This phase choice gives the most symmetric solution with the less spread of the Tb moment size with refined lengths of 4.75(3), 7.27(3), 8.75(4) and 3.26(3) μ_B.

Both solutions find the moments on each triangle sum to be $\pm$0.75 μ_B, which arrange into an emergent antiferromagnetic-like state, absent from nearest neighbour interactions alone.

This is analogous to the emergent charge order observed in the kagome ECO states, [17, 52] which has two observed experimental signatures; non-zero entropy and the presence of magnetic diffuse and Bragg-like peaks in the neutron diffraction measurements. [53] Such exotic magnetic states are elusive and have so far only been reported in oxide materials. Based on observing similar features this may be the first example of such a state present in a MOF. The emergence of antiferromagnetic order, associated with $\mathbf{k}_2$, is consistent with the observation of antiferromagnetic-like transitions in the physical property data. The emergent order present here does suggest that the 1D order of the TIA phase is retained in this lower temperature phase.

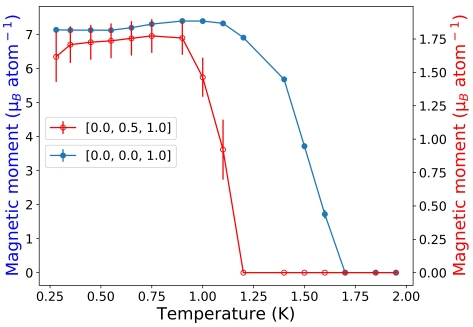

Figure 8. Evolution of the ordered magnetic moments associated with $\mathbf{k}_1$ and $\mathbf{k}_2$, in $Tb(DCO_2)_3$, with respect to temperature.

The evolution of the magnetic moments, with respect to temperature, associated with the two **k**-vectors is shown in Figure 8. Whilst the high temperature transition is consistent with the physical property measurements we attribute the low temperature transition discrepancy to temperature equilibration issues, in particular that the physical property measurements were measured on cooling and neutron diffraction patterns on warming.

(ii) $Ho(DCO_2)_3$

In all the samples studied, excluding $Tb(DCO_2)_3$, the only material which shows evidence of structured magnetic scattering is $Ho(DCO_2)_3$. $Ho(DCO_2)_3$ begins to exhibit diffuse scattering below 10 K, whilst remaining paramagnetic to 1.6 K, see Figures S2-25 for neutron diffraction patterns. The other samples did not show any magnetic diffuse scattering above 1.5 K. The diffuse in $Ho(DCO_2)_3$ has been fit well with SPINVERT, and the stereographic projections of the refined spin orientations indicate that the spins are preferentially aligned along the *c*-axis (see Figure 9a), consistent with large spin-orbit coupling and the Ising-like magnetic anisotropy, seen in $Tb(DCO_2)_3$. [9] Attempts were therefore made to fit the diffuse scattering data with Ising spins constrained to point along the *c*-axis. The Ising refinements also yielded a reasonable fit (Figure 9a), though of somewhat lower quality than the Heisenberg-like refinement (χ^2= 2.53 and 8.29), expected as the Ising refinement is more highly constrained compared to Heisenberg fits. This result suggests that the spins have a strong, although probably not purely, Ising character. These results are consistent with observed Ho^{+3} anisotropy seen in the spin-ice materials $Ho_2Ti_2O_7$ and $Ho_2Sn_2O_7$. [54] We would therefore expect to see a gap in the inelastic neutron spectra of $Ho(DCO_2)_3$ and $Tb(DCO_2)_3$, between the ground and first excited state.

Spin correlations $\langle S_0 \cdot S_r \rangle$, averaged over 100 RMC refinements, show that dominant spin correlations in this material are ferromagnetic along the chain direction, with weaker antiferromagnetic interchain interactions. We have extracted correlation lengths with the function $\langle S_0 \cdot S_r \rangle = Aexp(-r/\epsilon)$, where A is the Ising-like anisotropy, r is the correlation distance and ϵ is the correlation length. As the temperature was raised and the correlations became significantly

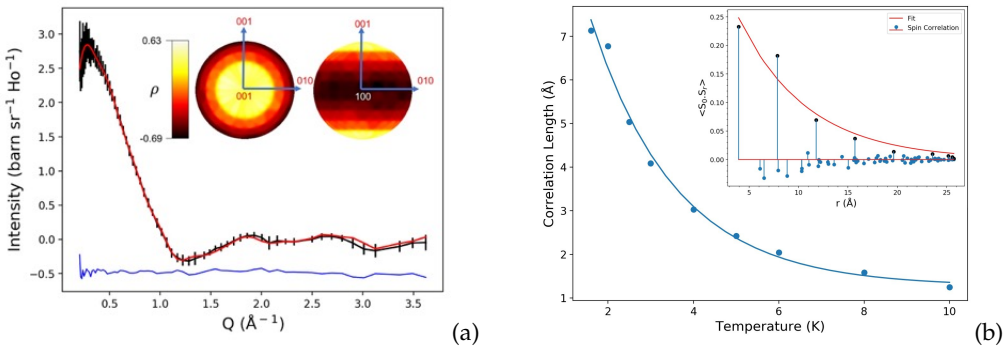

Figure 9. (a) RMC fit to magnetic diffuse with an Ising model, data points in black, fit in red and the difference in blue, and stereographic projections in insert. Stereographic projections of the spin orientations averaged over 100 RMC Heisenberg-like fits to diffuse neutron scattering data from $Ho(DCO_2)_3$ at 1.6 K. The relative spin density, $\rho(\theta,\phi)$, is defined as $\rho(\theta,\phi) = \ln\left[\frac{\rho(\theta,\phi)}{Nd(cos\theta)d\phi}\right]$ (b) correlation lengths at various temperature with spin correlations and fit of $Ho(DCO_2)_3$ at 1.6 K in insert with chain correlations highlighted in black.

weaker, the best fit to data was found with un-physical A values, for this reason A was fixed to the value - 0.72 - determined for the lowest temperature fit. For correlation fits see Figure S26.

At 1.6 K, the ferromagnetic chain correlation length is 7.3(6) Å with weaker antiferromagnetic inter-chain correlations of -0.018(2) and -0.034(2) observed for Ho^{3+} cations separated by 6.10 and 6.57 Å, found in triangles respectively. This indicates that the correlations in $Ho(DCO_2)_3$ are weaker than $Tb(DCO_2)_3$ for a given temperature. [44] In the *Ln*$(DCO_2)_3$ series $Tb(DCO_2)_3$ and $Ho(HCO_2)_3$ were both noted to have their magnetocaloric properties optimised for use above 4 K, these are also the only two compounds to show structured diffuse scattering above 1.6 K. $Ho(HCO_2)_3$ may be a worse magnetocaloric than $Tb(HCO_2)_3$ due to its weaker ferromagnetic correlations, needing greater changes in magnetic fields to align spins with the field. The decrease in correlation lengths in $Ho(DCO_2)_3$ follows the same exponential law seen in the $Tb(DCO_2)_3$ framework and the relative strength of the ferromagnetic intrachain and anitferromagnetic interchain correlations in the two compounds is the same. We therefore suggest at sufficiently low temperatures, it is likely that the $Ho(DCO_2)_3$ framework will feature similar exotic magnetic states to that of $Tb(DCO_2)_3$.

4. Conclusion

This work reports the physical properties and lower temperature magnetic structure of $Tb(DCO_2)_3$, and the magnetic correlations of $Ho(DCO_2)_3$ in the paramagnetic state. The magnetic phase observed in $Tb(DCO_2)_3$ below 1.2 K appears to display emergent order, when interpreted via conventional crystallographic approaches, in the long-range structure. This result is robust to the two possible magnetic structures which vary only in the phase of their scattering and as such it may be the first example of such a state in a MOF. The broadness of the Bragg-like peaks and retention of the magnetic diffuse scattering is consistent with the retention of 1D order in the TIA phase of $Tb(DCO_2)_3$ in this lower temperature phase. $Ho(DCO_2)_3$ shows significant magnetic diffuse scattering at 1.6 K, indicating the inherent magnetic frustration in this system. Fits to this suggest that it has similar magnetic correlations to that seen in the paramagnetic phase of $Tb(DCO_2)_3$ which suggests it may exhibit similar exotic phases at lower temperatures. The stronger 1D ferromagnetic correlations in $Tb(DCO_2)_3$ likely explain why this is the most efficient magnetocaloric material of the two compounds. This highlights the great potential for exotic magnetic states to emerge in MOFs, including new emergent phases.

Data Accessibility. Electronic supplementary material (ESM) is available online and neutron data can be downloaded from DOI:/10.5286/ISIS.E.86390259

Authors' Contributions. R.J.C.D carried out data analysis, and measurements, and drafted the manuscript. F.O and P.M provided assistance with Rietveld refinements and the neutron diffraction measurements. P.M and S.E.D collected physical property data, and assisted with analysis. P.J.S conceived and designed the study and drafted the manuscript. All authors read and approved the manuscript.

Competing Interests. The authors declare that they have no competing interests.

Funding. The authors would like to thank the Science and Technologies Facilities Council for access to the ISIS facility at Harwell. R.J.C.D would like to acknowledge the University of Kent's for financial support through the provision of a Vice-Chancellors scholarship. P.J.S would like to thank the Leverhulme Trust for funding via RPG-2018-268. P.M and S.E.D acknowledge funding from the Winton Programme for the Physics of Sustainability. Low temperature MPMS measurements were carried out on the EPSRC Advanced Materials Characterisation Suite (EP1M0052411).

Acknowledgements. R.J.C.D would like to thank J.A.M Paddison for his continued SPINVERT support.

References

1. Moessner R, Ramirez AP. 2006 Geometrical frustration.
Phys. Today **59**, 24–29.
(doi:10.1063/1.2186278)
2. Spaldin NA. 2010 *Magnetic materials: Fundamentals and applications*.
Cambridge: Cambridge University Press.
(doi:10.1017/CBO9780511781599)
3. Pecharsky VK, Gschneidner KA. 1999 Magnetocaloric effect and magnetic refrigeration.
J. Magn. Magn. Mater. **200**, 44–56.
(doi:10.1016/S0304-8853(99)00397-2)
4. Xiao YD, Paudel R, Liu J, Ma C, Zhang ZS, Zhou SK. 2016 MRI contrast agents: Classification and application (Review).
Int. J. Mol. Med. **38**, 1319–1326.
(doi:10.3892/ijmm.2016.2744)
5. Wasilewski P, Kletetschka G. 1999 Lodestone: Natures only permanent magnet-what it is and how it gets charged.
Geophys. Res. Lett. **26**, 2275–2278.
(doi:10.1029/1999GL900496)
6. Li JR, Kuppler RJ, Zhou HC. 2009 Selective gas adsorption and separation in metal-organic frameworks.
Chem. Soc. Rev. **38**, 1477–504.
(doi:10.1039/b802426j)
7. Yaghi OM, Li H, Davis C, Richardson D, Groy TL. 1998 Synthetic Strategies, Structure Patterns, and Emerging Properties in the Chemistry of Modular Porous Solids.
Acc. Chem. Res. **31**, 474–484.
(doi:10.1021/ar970151f)
8. Kreno LE, Leong K, Farha OK, Allendorf M, Van Duyne RP, Hupp JT. 2012 Metal-organic framework materials as chemical sensors.
Chem. Rev. **112**, 1105–1125.
(doi:10.1021/cr200324t)
9. Saines PJ, Paddison JAM, Thygesen PMM, Tucker MG. 2015 Searching beyond Gd for magnetocaloric frameworks: magnetic properties and interactions of the $Ln(HCO_2)_3$ series.
Mater. Horizons **2**, 528–535.
(doi:10.1039/c5mh00113g)
10. Dixey RJ, Saines PJ. 2018 Optimization of the Magnetocaloric Effect in Low Applied Magnetic Fields in $LnOHCO_3$ Frameworks.
Inorg. Chem. **57**, 12543–12551.
(doi:10.1021/acs.inorgchem.8b01549)
11. Jain P, Ramachandran V, Clark RJ, Hai DZ, Toby BH, Dalal NS, Kroto HW, Cheetham AK. 2009 Multiferroic behavior associated with an order-disorder hydrogen bonding transition in metal-organic frameworks (MOFs) with the perovskite ABX_3 architecture.

J. Am. Chem. Soc. **131**, 13625–13627.
(doi:10.1021/ja904156s)
12. Ising E. 1925 Beitrag zur Theorie des Ferromagnetismus.
Zeitschrift für Phys. **31**, 253–258.
(doi:10.1007/BF02980577)
13. Wannier GH. 1950 Antiferromagnetism. The triangular Ising net.
Phys. Rev. **79**, 357–364.
(doi:10.1103/PhysRev.79.357)
14. Castelnovo C, Moessner R, Sondhi S. 2012 Spin Ice, Fractionalization, and Topological Order.
Annu. Rev. Condens. Matter Phys. **3**, 35–55.
(doi:10.1146/annurev-conmatphys-020911-125058)
15. Castelnovo C, Moessner R, Sondhi SL. 2008 Magnetic monopoles in spin ice.
Nature **451**, 42–45.
(doi:10.1038/nature06433)
16. Paddison JA, Jacobsen H, Petrenko OA, Fernández-Díaz MT, Deen PP, Goodwin AL. 2015 Hidden order in spin-liquid $Gd_3Ga_5O_{12}$.
Science **350**, 179–181.
(doi:10.1126/science.aaa5326)
17. Paddison JA, Ong HS, Hamp JO, Mukherjee P, Bai X, Tucker MG, Butch NP, Castelnovo C, Mourigal M, Dutton SE. 2016 Emergent order in the kagome Ising magnet $Dy_3Mg_2Sb_3O_{14}$.
Nat. Commun. **7**, 13842.
(doi:10.1038/ncomms13842)
18. Serrano-González H, Bramwell ST, Harris KDM, Kariuki BM, Nixon L, Parkin IP, Ritter C. 1999 Structural and magnetic characterization of the frustrated triangular-lattice antiferromagnets $CsFe(SO_4)_2$ and $RbFe(SO_4)_2$.
Phys. Rev. B **59**, 14451–14460.
(doi:10.1103/PhysRevB.59.14451)
19. Kawamura, H Miyashita S. 1985 Phase Transitions of Anisotropic Heisenberg Antiferromagnets on the Triangular Lattice.
J. Phys. Soc. Japan **54**, 3385–3395.
(doi:10.1143/JPSJ.54.3385)
20. Keen DA, Goodwin AL. 2015 The crystallography of correlated disorder.
Nature **521**, 303–309.
(doi:10.1038/nature14453)
21. Mendels P, Bert F. 2016 Quantum kagome frustrated antiferromagnets: One route to quantum spin liquids.
Comptes Rendus Phys. **17**, 455–470.
(doi:10.1016/j.crhy.2015.12.001)
22. Norman MR. 2016 Colloquium: Herbertsmithite and the search for the quantum spin liquid.
Rev. Mod. Phys. **88**, 041002.
(doi:10.1103/RevModPhys.88.041002)
23. Helton JS, Matan K, Shores MP, Nytko EA, Bartlett BM, Yoshida Y, Takano Y, Suslov A, Qiu Y, Chung JH, Nocera DG, Lee YS. 2007 Spin dynamics of the spin-1/2 kagome lattice antiferromagnet $ZnCu_3(OH)_6Cl_2$.
Phys. Rev. Lett. **98**, 107204.
(doi:10.1103/PhysRevLett.98.107204)
24. Banerjee A, Bridges CA, Yan JQ, Aczel AA, Li L, Stone MB, Granroth GE, Lumsden MD, Yiu Y, Knolle J, Bhattacharjee S, Kovrizhin DL, Moessner R, Tennant DA, Mandrus DG, Nagler SE. 2016 Proximate Kitaev quantum spin liquid behaviour in a honeycomb magnet.
Nat. Mater. **15**, 733–740.
(doi:10.1038/nmat4604)
25. Majorana E. 1937 Teoria simmetrica dell'elettrone e del positrone.
Nuovo Cim. **14**, 171–184.
(doi:10.1007/BF02961314)
26. Paddison JA, Daum M, Dun Z, Ehlers G, Liu Y, Stone MB, Zhou H, Mourigal M. 2017 Continuous excitations of the triangular-lattice quantum spin liquid $YbMgGaO_4$.
Nat. Phys. **13**, 117–122.
(doi:10.1038/nphys3971)

27. Mitra C. 2015 Spin chains: Long-distance relationship.
Nat. Phys. **11**, 212–213.
(doi:10.1038/nphys3249)
28. Koretsune T, Ogata M. 2002 Resonating-valence-bond states and ferromagnetic correlations in the doped triangular mott insulator.
Phys. Rev. Lett. **89**, 116401.
(doi:10.1103/PhysRevLett.89.116401)
29. Peierls R. 1936 On Ising's model of ferromagnetism.
Math. Proc. Cambridge Philos. Soc. **32**, 477–481.
(doi:10.1017/S0305004100019174)
30. Blundell S. 2001 *Magnetism in Condensed Matter*, volume 71.
Oxford University Press.
(doi:10.1088/1751-8113/44/8/085201)
31. Vasiliev A, Volkova O, Zvereva E, Markina M. 2018 Milestones of low-D quantum magnetism.
npj Quantum Mater. **3**, 18.
(doi:10.1038/s41535-018-0090-7)
32. Yoshizawa H, Kozukue W, Hirakawa K. 1980 Neutron Scattering Study of Magnetic Excitations in Pseudo-One-Dimensional Singlet Ground State Ferromagnets $CsFeCl_3$ and $RbFeCl_3$.
J. Phys. Soc. Japan **49**, 144–153.
(doi:10.1143/JPSJ.49.144)
33. Mekata M, Sugino A Oohara AT, Ohara Yasuda Y Oohara H Yoshizawa KS. 1995 Magnetic ordering in $CsCuCl_3$.
J. Magn. Magn. Mater. **140-144**, 1987–1988.
(doi:10.1016/0304-8853(94)01177-X)
34. Kakurai K, Pynn R, Dorner B, Steiner M. 1984 A polarised neutron study of linear and non-linear spin fluctuations in $CsNiF_3$.
J. Phys. C Solid State Phys. **17**, L123–L128.
(doi:10.1088/0022-3719/17/4/002)
35. Nguyen TN, Lee PA, Zur Loye HC. 1996 Design of a random quantum spin chain paramagnet: $Sr_3CuPt_{0.5}lr_{0.5}O_6$.
Science **271**, 489–491.
(doi:10.1126/science.271.5248.489)
36. Maignan A, Hardy V, Hébert S, Drillon M, Lees MR, Petrenko O, Paul DMK, Khomskii D. 2004 Quantum tunneling of the magnetization in the Ising chain compound $Ca_3Co_2O_6$.
J. Mater. Chem. **14**, 1231–1234.
(doi:10.1039/b316717h)
37. Paddison JA, Agrestini S, Lees MR, Fleck CL, Deen PP, Goodwin AL, Stewart JR, Petrenko OA. 2014 Spin correlations in $Ca_3Co_2O_6$: Polarized-neutron diffraction and Monte Carlo study.
Phys. Rev. B **90**, 014411.
(doi:10.1103/PhysRevB.90.014411)
38. Nandi M, Mandal P. 2016 Magnetic and magnetocaloric properties of quasi-one-dimensional Ising spin chain CoV_2O_6.
J. Appl. Phys. **119**, 133904.
(doi:10.1063/1.4945395)
39. Paddison JAM, Goodwin AL. 2012 Empirical magnetic structure solution of frustrated spin systems.
Phys. Rev. Lett. **108**, 017204.
(doi:10.1103/PhysRevLett.108.017204)
40. Paddison JAM, Ross Stewart J, Goodwin AL. 2013 spinvert: a program for refinement of paramagnetic diffuse scattering data.
J. Phys. Condens. Matter **25**, 454220.
(doi:10.1088/0953-8984/25/45/454220)
41. Saines PJ, Bristowe NC. 2018 Probing magnetic interactions in metal–organic frameworks and coordination polymers microscopically.
Dalt. Trans. **47**, 13257–13280.
(doi:10.1039/C8DT02411A)
42. Gutschke SOH, Molinier M, Powell AK, Wood PT. 1997 Hydrothermal Synthesis

of Microporous Transition Metal Squarates: Preparation and Structure of $[Co_3(\mu_3\text{-}OH)_2(C_4O_4)_2]\cdot 3H_2O$.
Angew. Chemie Int. Ed. English **36**, 991–992.
(doi:10.1002/anie.199709911)

43. Feyerherm R, Loose A, Manson JL. 2003 Unusual magnetic-field dependence of partially frustrated triangular ordering in manganese tricyanomethanide.
J. Phys. Condens. Matter **15**, 663–673.
(doi:10.1088/0953-8984/15/4/307)
44. Harcombe DR, Welch PG, Manuel P, Saines PJ, Goodwin AL. 2016 One-dimensional magnetic order in the metal-organic framework $Tb(HCOO)_3$.
Phys. Rev. B **94**, 174429.
(doi:10.1103/PhysRevB.94.174429)
45. Chapon LC, Manuel P, Radaelli PG, Benson C, Perrott L, Ansell S, Rhodes NJ, Raspino D, Duxbury D, Spill E, Norris J. 2011 Wish: The New Powder and Single Crystal Magnetic Diffractometer on the Second Target Station.
Neutron News **22**, 22–25.
(doi:10.1080/10448632.2011.569650)
46. Rodríguez-Carvajal J. 1993 Recent advances in magnetic structure determination by neutron powder diffraction.
Phys. B Phys. Condens. Matter **192**, 55–69.
(doi:10.1016/0921-4526(93)90108-I)
47. Petrícek V, Dušek M, Palatinus L. 2014.
Crystallographic computing system JANA2006: General features.
(doi:10.1515/zkri-2014-1737)
48. Rietveld HM. 1969 A profile refinement method for nuclear and magnetic structures.
J. Appl. Crystallogr. **2**, 65–71.
(doi:10.1107/S0021889869006558)
49. Kurbakov A, Rodríquez-Carvajal J, Trounov V, Starostina N. 2000 Discovery and Investigation of the Magnetic Structure of Terbium Formate $Tb(DCOO)_3$.
Mater. Sci. Forum **321-324**, 971–975.
(doi:10.4028/www.scientific.net/MSF.321-324.971)
50. Wills AS, Oakley GS, Visser D. and Frunzke J, Harrison A. and Andersen, KH. 2001 Short-range order in the topological spin glass $(D_3O)Fe_3(SO_4)_2(OD)_6$ using xyz polarized neutron diffraction.
Phys. B Phys. Condens. Matter **9**, 094436.
(doi:10.1103/PhysRevB.64.094436)
51. Campbell BJ, Stokes HT, Tanner DE, Hatch DM. 2006 ISODISPLACE: A web-based tool for exploring structural distortions.
J. Appl. Crystallogr. **39**, 607–614.
(doi:10.1107/S0021889806014075)
52. Fennell T, Bramwell ST, McMorrow DF, Manuel P, Wildes AR. 2007 Pinch points and Kasteleyn transitions in kagome ice.
Nat. Phys. **3**, 566–572.
(doi:10.1038/nphys632)
53. Canals B, Chioar IA, Nguyen VD, Hehn M, Lacour D, Montaigne F, Locatelli A, Menteş TO, Burgos BS, Rougemaille N. 2016 Fragmentation of magnetism in artificial kagome dipolar spin ice.
Nat. Commun. **7**, 11446.
(doi:10.1038/ncomms11446)
54. Bramwell, ST. and Gingras, MJP. 2001 Spin ice state in frustrated magnetic pyrochlore materials.
Science **294**, 1495.
(doi:10.1126/science.1064761)